

Quantum diffusion map for nonlinear dimensionality reduction

Apimuk Sornsang, Ninnat Dangniam, Pantita Palittapongarnpim,* and Thiparat Chotibut†

*Chula Intelligent and Complex Systems, Department of Physics,
Faculty of Science, Chulalongkorn University, Bangkok, Thailand, 10330*

(Dated: June 15, 2021)

Inspired by random walk on graphs, diffusion map (DM) is a class of unsupervised machine learning that offers automatic identification of low-dimensional data structure hidden in a high-dimensional dataset. In recent years, among its many applications, DM has been successfully applied to discover relevant order parameters in many-body systems, enabling automatic classification of quantum phases of matter. However, classical DM algorithm is computationally prohibitive for a large dataset, and any reduction of the time complexity would be desirable. With a quantum computational speedup in mind, we propose a quantum algorithm for DM, termed *quantum diffusion map* (qDM). Our qDM takes as an input N classical data vectors, performs an eigen-decomposition of the Markov transition matrix in time $O(\log^3 N)$, and classically constructs the diffusion map via the readout (tomography) of the eigenvectors, giving a total runtime of $O(N^2 \text{polylog } N)$. Lastly, quantum subroutines in qDM for constructing a Markov transition operator, and for analyzing its spectral properties can also be useful for other random walk-based algorithms.

I. INTRODUCTION

Discovering statistical structure in high-dimensional data is essential for data-driven science and engineering. Advances in unsupervised machine learning offer a plethora of alternatives to automatically search for low-dimensional structure of data lying in a high-dimensional space. Many of these approaches involve dimensionality reduction. Classic approach is the principal component analysis (PCA), which projects high-dimensional data onto a low-dimensional linear space spanned by a set of orthonormal bases, whose directions capture significant data variations. More compelling approach enables automatic searches for a low-dimensional data manifold embedded in a high-dimensional space. Well-known manifold learning algorithms include Isomap [1], Laplacian eigenmaps [2], uniform manifold approximation and projection (UMAP) [3], nonlinear PCA [4], t-distributed stochastic neighbor embedding (t-SNE) [5], and diffusion map (DM) [6–8], which is the focus of this paper. Inspired by appealing features of random walk on graphs, DM and its variants have received increasing attention for data visualization in bioinformatics [9, 10]. DM has also recently been successfully applied to provide automatic classification of topological phases of matter, and offers automatic identification of quantum phase transitions in many-body systems [11–16].

Most dimensionality reduction methods require the computation of singular value decomposition (SVD) of a matrix constructed from a collection of high-dimensional data points. For a matrix of size, say, $N \times d$, where N is the number of data points and d is the dimensionality of each data vector (assumed to be smaller than N), the computational cost of SVD typically grows

with the number of data points as $O(N^3)$. Thus, classical dimensionality reduction can be computationally prohibitive for a large data sample. However, under moderate assumptions of accessibility to certain features of full-scale quantum computers, matrix exponentiation-based quantum algorithms have been proposed to perform SVD more efficiently [17]. In particular, assuming accessibility to appropriate quantum RAM, quantum singular value decomposition (qSVD) algorithm’s runtime for many non-sparse low-rank Hermitian matrices is $O(\text{polylog } N)$, which is exponentially faster than the classical counterpart and can be extended to non-square matrices. A classic quantum algorithm for dimensionality reduction with quantum computational speedup is quantum principal component analysis (qPCA), which exploits matrix exponentiation tricks as in qSVD [18]. More recently, quantum algorithms with quantum advantage for nonlinear dimensionality reduction and cluster identification based on spectral graph theory have also been proposed [19–21].

With a quantum computational speedup for dimensionality reduction in mind, we propose a quantum algorithm for unsupervised manifold learning called quantum diffusion map (qDM). Under mild assumptions of appropriate oracles, qDM has a runtime of roughly $O(\kappa_D^{1.25} N^2 \text{polylog } N)$ where N is the number of data points and κ_D is the condition number of the degree matrix (see Theorem 1 for the precise statement), as opposed to $O(N^3)$ in classical DM. Although κ_D depends strongly on the data structure and can take the value N in the worst case, such worst-case is highly atypical for well structured dataset. Without the final readout step, our qDM algorithm prepares all necessary components for constructing diffusion map in $O(\kappa_D^{1.25} \log^3 N)$ time.

Although the backbone of DM is a graph-based dimensionality reduction method, the procedure is different from other spectral graph methods. Namely, rather than working with the data-induced graph Laplacian as in Laplacian eigenmaps or in spectral clustering, DM

* Correspondence to panpalitta@gmail.com

† Correspondence to thiparatc@gmail.com, thiparat.c@chula.ac.th

involves Markov transition matrix that defines random walks on a data-induced graph. Therefore, recipes for qDM dimensionality reduction are different from the recently proposed quantum spectral clustering [19, 20].

The paper is organized as follows. Section II provides necessary ingredients to understand classical diffusion map and its runtime. Section III introduces quantum subroutines for qDM, which is then discussed in details in Section IV and V. qDM runtime complexity appears in Section VI. We conclude with the discussion and outlook in Section VII. Additional details on the algorithmic complexity and the subroutines for qDM are provided in Appendix A and B.

II. CLASSICAL DIFFUSION MAP FOR DIMENSIONALITY REDUCTION

Given a set of N data vectors $X \equiv \{\mathbf{x}^{(i)}\}_{i=0}^{N-1}$, in which each data vector has d features (i.e. $\mathbf{x}^{(i)} \in \mathbb{R}^d$), unsupervised machine learning seeks to identify the structure of data distribution in a high-dimensional ($d \gg 1$) space. When the data distribution has a highly nonlinear structure, classic linear approach such as PCA fails. Rather than using mere Euclidean distance as a similarity measure between data points, manifold learning approach assigns the connectivity among data points in their neighborhood as a proxy for proximity between points; e.g., points on a toroidal helix embedded in 3 dimensions with equal Euclidean distance can have different geodesic distances on a manifold (different similarity), see Fig. 1 (top). This approach allows one to perform a nonlinear dimensionality reduction by assigning an appropriate function that maps a high-dimensional data point into a relevant lower-dimensional Euclidean space embedding, while encapsulating the notion of proximity in high dimensions based on neighborhood connectivity.

Neighborhood connectivity leads to the development of graph-based manifold learning approach, where one can assign a vertex i to a data vector $\mathbf{x}^{(i)}$ and assign an edge between a pair of data points that are considered to be neighbors. Isomap [1] and Laplacian eigenmaps [2] are among the first graph-based manifold learning algorithms, where relevant low-dimensional data embedding can be extracted from eigen-decomposition of data-induced graph Laplacian matrix.

A. Diffusion map in a nutshell

In diffusion map (DM), the similarity matrix between a pair of data vectors, or equivalently the weighted edge between a pair of graph vertices, is often taken to be a Gaussian kernel:

$$W_{ij} \equiv K_\sigma(\mathbf{x}^{(i)}, \mathbf{x}^{(j)}) = \exp\left(-\frac{\|\mathbf{x}^{(i)} - \mathbf{x}^{(j)}\|_2^2}{2\sigma}\right), \quad (1)$$

where the adjustable parameter σ , called the *bandwidth*, sets the scale of neighborhood. Two points whose squared distance exceed this bandwidth contribute exponentially little to the weighted edge, suggesting that these two points are far away from being a neighbor in its original feature space. Given a graph with weighted edges W_{ij} 's, DM assigns a discrete-time random walk on a data-induced graph, where the Markov transition probability from vertex i to j is given by the normalized weighted edge,

$$P_{ij} = \frac{W_{ij}}{\sum_{j=0}^{N-1} W_{ij}}. \quad (2)$$

One can compactly compute the Markov transition matrix P from the (weighted) *adjacency matrix* W , and the *degree matrix* $D \equiv \text{diag}\{d_i\}_{i=0}^{N-1}$ where $d_j \equiv \sum_{i=0}^{N-1} W_{ij}$ by

$$P = D^{-1}W. \quad (3)$$

The notion of proximity based on graph connectivity can be characterized by how fast random walkers on a graph starting at different data points visit each other. One expects that two points that are connected by multiple paths should be near; whereas two points that are sparsely connected should lie far from each other. In fact, it can be shown that [8] the proper distance function, called *diffusion distance*, between two points $\mathbf{x}^{(i)}$ and $\mathbf{x}^{(j)}$ after a t -step random walk is given by

$$\text{Dist}_t^2(\mathbf{x}^{(i)}, \mathbf{x}^{(j)}) = \sum_{k=0}^{N-1} \frac{[(P^t)_{ik} - (P^t)_{jk}]^2}{u_0(\mathbf{x}^{(k)})}, \quad (4)$$

where u_0 is the *left* eigenvector with eigenvalue $\lambda_0 = 1$ of P and $u_0(\mathbf{x}^{(k)})$ denotes the k^{th} coordinate of u_0 .

Before obtaining a relevant lower-dimensional Euclidean space representation of the original data point $\mathbf{x}^{(i)}$, we first note the following important identity. Define the *diffusion map* with m bases as

$$\phi_{t,m}(\mathbf{x}^{(i)}) = \begin{pmatrix} \lambda_1^t v_1(\mathbf{x}^{(i)}) \\ \vdots \\ \lambda_m^t v_m(\mathbf{x}^{(i)}) \end{pmatrix}, \quad (5)$$

where v_i is the *right* eigenvector of P with eigenvalue λ_i , $v_i(\mathbf{x}^{(j)})$ denotes the j^{th} coordinate of v_i , and the eigenvalues are ordered such that $\lambda_0 = 1 > \lambda_1 \geq \lambda_2 \geq \dots \geq \lambda_{N-1} \geq 0$ assuming no degeneracy in the largest eigenvalue (which is always possible given σ is sufficiently large). Note that $\lambda_0 = 1$ is always the eigenvalue of a Markov transition matrix P with a normalized eigenvector $(1 \dots 1)^T/N$, corresponding to the stationary uniform distribution over all vertices. Then, the diffusion distance (4) can be *exactly* computed from the Euclidean representation in (5) with $m = N - 1$ bases [8];

$$\text{Dist}_t^2(\mathbf{x}^{(i)}, \mathbf{x}^{(j)}) = \left\| \phi_{t,N-1}(\mathbf{x}^{(i)}) - \phi_{t,N-1}(\mathbf{x}^{(j)}) \right\|_2^2. \quad (6)$$

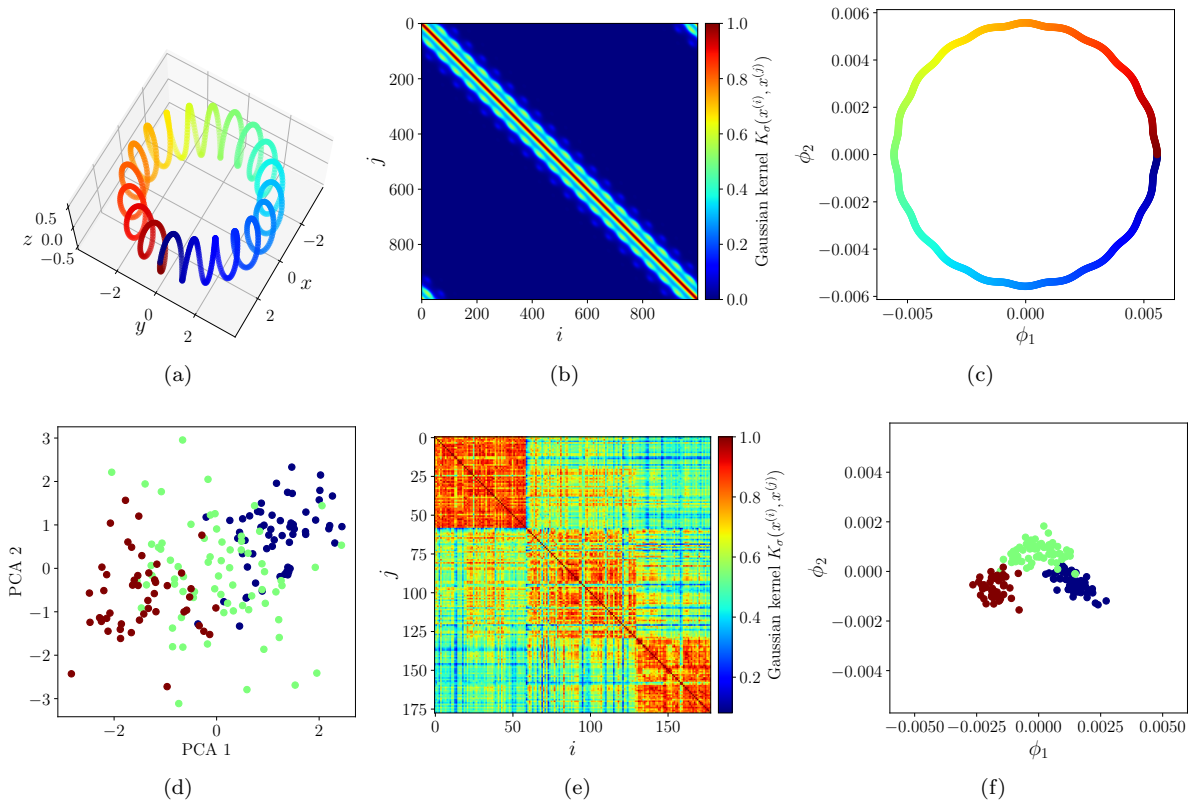


FIG. 1. The application of classical DM for nonlinear dimensionality reduction: (top) to identify the proximity structure of data points distributed as a toroidal helix in 3 dimensions, and (bottom) to reveal the proximity structure of 13 chemical components' concentrations of 178 wines ($d = 13, N = 178$) derived from 3 different cultivars grown in the same region in Italy, taken from the WINE dataset in [22]. In a toroidal helix data (top left), color variation signifies difference in the geodesic distance between points on a one-dimensional manifold. The Gaussian kernel with $\sigma = 1$ of (1) shows the neighborhood connectivity has a local, periodic structure (top middle). The dimensionality reduction (top right) into the first two components ($m = 2$) of the DM in (5) reveals a one-dimensional structure with an appropriate notion of geodesic distance (see color variations). In WINE dataset, wines grown from 3 different cultivars are labeled in 3 different colors (red, green, blue). Projecting the 13 data features (chemical concentrations) of all wines into the first two principal components using PCA does not suffice to distinguish the 3 types (bottom left). However, with the Gaussian kernel with $\sigma = 50$ (bottom middle), DM with two bases ($m = 2$) can reveal quite a clear distinction between types (bottom right). In addition, the proximity structure also suggests that the green type has its chemical components closer to those of the other two types. In both dataset, we use $t = 1$ in the DM. Thus, random walk on data-induced graphs can reveal salient low-dimensional data structure within just a one-step walk, provided σ is chosen appropriately.

The above equality states that the distance in the diffusion space (based on graph connectivity) is identical to the Euclidean embedding distance (induced by the diffusion map). Thus, the notion of proximity between data points from its graph connectivity can be simply computed from the Euclidean embedding by the diffusion map (5).

What about dimensionality reduction? Since P is a Markov transition matrix, its eigenvalues are $\lambda_0 = 1 \geq \lambda_1 \geq \lambda_2 \geq \dots \geq \lambda_{N-1} \geq 0$. Bases in (5) with low-lying eigenvalues are then exponentially suppressed as t -step increases. In the long-time limit, dimensionality reduction thus naturally arises in DM. One may take the number of bases m in (5) corresponding to the number of top eigenvalues of P , and still obtain meaningful low-dimensional Euclidean representation of points in the dif-

fusion space. In practice, for the purpose of visualization, taking $m = 2 \ll d$ is a drastic dimensionality reduction, yet DM with such small number of bases can yield insights into the approximate proximity of data in the original high-dimensional space, see Fig. 1. Using DM (5) to extract low-dimensional data representation that approximately preserves the notion of distance from neighborhood connectivity in the original high-dimensional space is also the first step towards data clustering algorithms. Namely, one may employ standard clustering algorithms, such as k-means algorithm, on the low-dimensional outputs of the DM without suffering from the curse of dimensionality problem.

B. Time complexity of classical diffusion map

Numerical recipes to obtain nonlinear dimensionality reduction or manifold learning in classical DM consists of 4 steps:

1. Construct the data-induced similarity matrix (weighted adjacency matrix) W from (1)
2. Construct the Markov transition matrix P from (3); i.e. $P = D^{-1}W$
3. Compute the eigen-decomposition of P
4. Construct the diffusion map (5)

We now discuss the time complexity for each step as a function of the number of data points N . Assuming the Gaussian kernel function (1), the weighted adjacency matrix W is symmetric. The number of the elements that the algorithm needs to calculate is then $\sum_{i=1}^N i = (N^2 + N)/2$. Therefore, the time complexity of calculating the kernel matrix in step 1 is $O(N^2)$.

For step 2, the calculation of P involves normalizing each row of W as in (2). Numerical computation of the normalization factor, which is simply the summation, takes the time $O(N)$. Then normalizing each row costs another $O(N)$. Applying these procedures over the $N \times N$ matrix thus yields the time cost $O(N^2) + O(N^2)$. Hence, the time complexity for computing P is $O(N^2)$.

In step 3, the time cost stems from finding $\{v_i\}$ and $\{\lambda_i\}$ of P , using singular value decomposition (SVD), which can be applied to any non-squared matrices. This algorithm comprises two steps [23]. The first step is to use Householder transformations to reduce P to a bidiagonal form. Then the QR algorithm is applied to find singular values. The time complexity of these two steps combined is $O(N^3)$.

The last step is computing the diffusion map ϕ according to (5), which involves the multiplication of λ_i^t with its corresponding right eigenvector v_i . Although we might not need to perform the multiplication for all $N - 1$ right eigenvectors as some λ_i^t maybe negligible in the long-time limit, we consider the worst case scenario where all $N - 1$ eigenvectors are required. With the length of each vector being N , the time cost is $O(N^2 - N)$ for computing ϕ and thus the time complexity for this step is $O(N^2)$.

Combining all the steps above, which is implemented in sequence, classical DM has a time complexity of $O(N^2) + O(N^2) + O(N^3) + O(N^2)$ leading to an overall time complexity that scales as $O(N^3)$. Note here that the time complexity is primarily dominated by the eigen-decomposition algorithm, which is subjected to change if a different algorithm is chosen in the implementation. In fact, this dominating complexity of $O(N^3)$ from eigen-decomposition urges for the development of quantum algorithms to achieve a quantum computational speedup, which we discuss next.

III. QUANTUM DIFFUSION MAP ROADMAP

In this section, we first give an outline of qDM algorithm summarized in Fig. 2. Then we proceed with classical to quantum data encoding, and the construction of the kernel matrix in Sec. III A and Sec. III B, respectively. Constructing the Markov transition matrix P and extracting relevant eigen-decomposition of P are not straightforward, and will be discussed in the following Sec. IV and Sec. V, respectively.

From now on, we will focus on the case where the weighted adjacency matrix is the Gaussian kernel matrix, so that $W = K$. To reduce the dominating complexity in the construction of the diffusion map, we first turn to the idea of quantum mechanically encoding the (normalized) kernel matrix a density matrix \hat{K} without explicitly evaluating each matrix element. Using the fact that the Gaussian kernel (1) is the inner product of canonical coherent states, this can be done in $O(\log N)$ time assuming quantum random access memory (qRAM) by exploiting ‘‘quantum parallelism’’, the ability to query data in superposition.

To construct the transition matrix, our algorithm uses as subroutines density matrix exponentiation [18], quantum matrix algebra toolbox (QMAT) [24], and quantum matrix inversion [25, 26]. While it is straightforward to compute the degree matrix D given elements of K , here we do not have direct access to elements of the density matrix \hat{K} without performing full tomography. Instead, we compute D via the identity

$$D = (K \mathbb{1}) \odot I, \quad (7)$$

where \odot is element-wise multiplication also known as Hadamard product, $\mathbb{1}$ is the all-ones matrix, and I is the identity matrix. Such matrix arithmetics can be done in the QMAT framework given the exponential of the relevant matrices either by density matrix exponentiation for \hat{K} , or Hamiltonian simulation to exponentiate sparse matrices [27]. We then use quantum phase estimation (QPE) to invert D akin to the HHL algorithm [25], compute $P \equiv D^{-1}K$, and use the QPE again to extract the eigenvalues and (right) eigenvectors of P . The diffusion map is then constructed classically. The time complexity is given in Section VI.

A. Quantum state encoding into coherent states

By the fact that the Gaussian kernel arises naturally as the inner product of coherent states, ref. [28] proposed encoding classical data into multi-mode coherent states

$$\mathbf{x}^{(i)} \mapsto \left| \mathbf{x}^{(i)} \right\rangle = \bigotimes_{p=0}^{d-1} \left| x_p^{(i)} \right\rangle, \quad (8)$$

where each single-mode coherent state $\left| x_p^{(i)} \right\rangle$ represents the p^{th} feature of datum $\mathbf{x}^{(i)}$. In continuous-variable

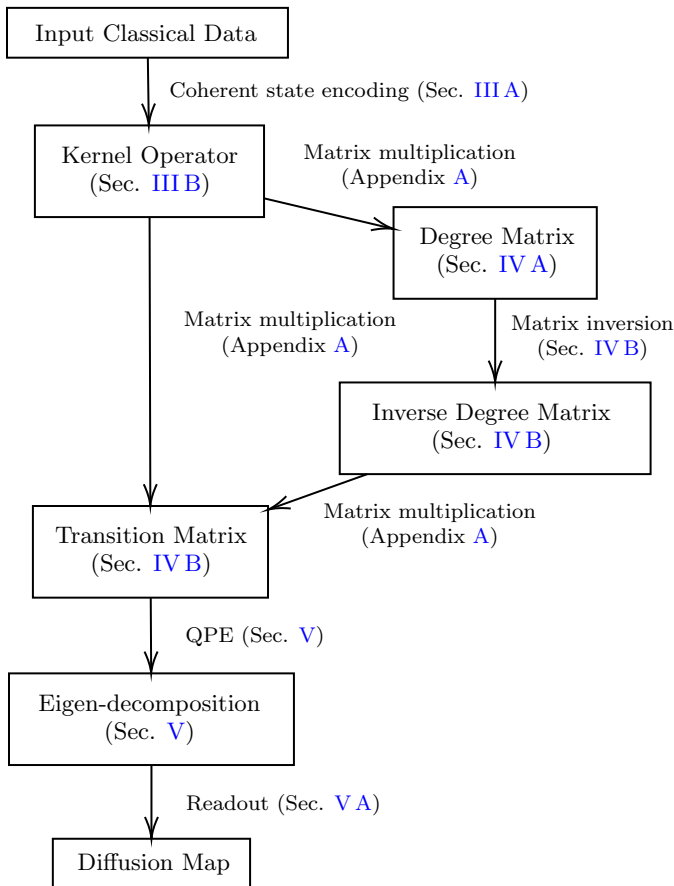


FIG. 2. The roadmap for quantum diffusion map algorithm.

quantum systems, the canonical coherent states are states with minimal and equal uncertainties in both quadratures. They are displaced ground state of the harmonic oscillator, and can be realized, for example, as the state of classical electromagnetic radiation. A single-mode coherent state is defined as

$$|x_p^{(i)}\rangle = \exp\left(-\frac{(x_p^{(i)})^2}{2}\right) \sum_{n=0}^{\infty} \frac{(x_p^{(i)})^n}{\sqrt{n!}} |n\rangle, \quad (9)$$

where $|n\rangle$ is the n^{th} eigenstate of the harmonic oscillator.

The inner product between two data vectors is the Gaussian kernel

$$\begin{aligned} \langle \mathbf{x}^{(i)} | \mathbf{x}^{(j)} \rangle &= \prod_{p=0}^{d-1} \langle x_p^{(i)} | x_p^{(j)} \rangle \\ &= \prod_{p=0}^{d-1} \exp\left(-\frac{(x_p^{(i)} - x_p^{(j)})^2}{2}\right) \\ &= \exp\left(-\frac{\|\mathbf{x}^{(i)} - \mathbf{x}^{(j)}\|_2^2}{2}\right) = K(\mathbf{x}^{(i)}, \mathbf{x}^{(j)}). \end{aligned} \quad (10)$$

Here, we take $\sigma = 1$ for simplicity (though σ can be incorporated by a scaling factor during state encoding in classical pre-processing). Recall that we focus on the kernel matrix as the weight matrix, and thus we denote K for describing the weight matrix W .

B. Kernel matrix

Now we exploit superposition access to the encoded data to implicitly evaluate the kernel matrix. This can be done efficiently assuming qRAM for instance [29]. Calling the oracle with the state $\frac{1}{\sqrt{N}} \sum_{i=0}^{N-1} |i\rangle$ entangles the data vectors with their labels:

$$|\psi\rangle = \frac{1}{\sqrt{N}} \sum_{i=0}^{N-1} |i\rangle_{\text{label}} \otimes |\mathbf{x}^{(i)}\rangle_{\text{position}}. \quad (11)$$

The reduced density matrix of the label space is given by the partial trace over the position space:

$$\begin{aligned} \text{Tr}_{\text{position}}(|\psi\rangle\langle\psi|) &= \frac{1}{N} \sum_{i,j=0}^{N-1} \langle \mathbf{x}^{(i)} | \mathbf{x}^{(j)} \rangle |i\rangle\langle j| \\ &= \frac{1}{N} \sum_{i,j=0}^{N-1} K(\mathbf{x}^{(i)}, \mathbf{x}^{(j)}) |i\rangle\langle j| \\ &= \frac{K}{N} \equiv \hat{K}, \end{aligned} \quad (12)$$

where $\text{Tr}(\hat{K}) = \sum_{i=0}^{N-1} K(\mathbf{x}^{(i)}, \mathbf{x}^{(i)}) = N$. Copies of \hat{K} will be used to prepare the degree matrix and the transition matrix.

IV. QUANTUM SUBROUTINE FOR CALCULATING THE TRANSITION MATRIX

In this section, we show that the degree matrix and its inverse, and consequently the transition matrix, can be obtained efficiently in a coherent fashion. In particular, if one can efficiently perform matrix multiplication and Hadamard product \odot involving \hat{K} , then one can efficiently obtain the degree matrix according to (7). Such matrix arithmetics can be done in the QMAT framework [24] by first exponentiating the relevant (possibly non-Hermitian) matrices A in the form $e^{iX_i(A)}$, where

$$X_i(A) = R_i \otimes A + R_i^\dagger \otimes A^\dagger, \quad (13)$$

and

$$R_1 = |0\rangle\langle 1|, \quad R_2 = |1\rangle\langle 2|, \quad R_3 = |0\rangle\langle 2|, \quad (14)$$

are qutrit operators. Once one has the ability to apply, say, $e^{iX_1(A_1)}$ and $e^{iX_2(A_2)}$ (shuffling between $R_i, i = 1, 2, 3$ can be done by a simple permutation of the qutrit basis states), then using the commutation relation between $X_1(A_1)$ and $X_2(A_2)$ one can approximate $e^{iX_3(A_3)}$ where A_3 is the result of the desired binary operation between A_1 and A_2 .

A. Calculate the exponential of degree matrix

To compute the degree matrix, we require QMAT sub-routines for (i) matrix multiplication, (ii) tensor product, and (iii) Hadamard product. The latter two sub-routines reduce to matrix multiplication as $A_1 \otimes A_2 = (A_1 \otimes I)(I \otimes A_2)$, and

$$\Xi(A_1 \otimes A_2)\Xi^\dagger = (A_1 \odot A_2) \otimes |0\rangle\langle 0|, \quad (15)$$

where

$$\Xi = \sum_{i=0}^{N-1} |i\rangle\langle i| \otimes |\mathbf{0}\rangle\langle i|, \quad (16)$$

and $|\mathbf{0}\rangle = |0 \cdots 0\rangle$ [24]. The multiplication subroutine and its complexity is summarized in Appendix A.

Define the (rank-one) density matrix

$$\hat{\mathbb{1}} \equiv \frac{1}{N} \sum_{i,j=0}^{N-1} |i\rangle\langle j| = \frac{\mathbb{1}}{N}. \quad (17)$$

If $e^{iX_i(\hat{K})\tau}$, $e^{iX_i(\hat{\mathbb{1}})\tau}$, $e^{iX_i(\Xi)\tau}$ and $e^{iX_i(\Xi^\dagger)\tau}$ can be constructed efficiently for some time τ , then one can construct for a larger time t (to be determined later for the purpose of phase estimation) the controlled- $e^{iX_3(\hat{D})t}$ unitary

$$\begin{aligned} e^{iX_3(\Xi(\hat{K}\hat{\mathbb{1}}\otimes I)\Xi^\dagger)t} &= e^{iX_3(\hat{D})t} \otimes |\mathbf{0}\rangle\langle \mathbf{0}| + I \otimes (I - |\mathbf{0}\rangle\langle \mathbf{0}|) \\ &\equiv \mathcal{U}_D. \end{aligned} \quad (18)$$

The last register will be discarded in the inversion step.

Now we discuss efficient construction of the unitary matrices required in the above procedure. Ξ is sparse and thus can be exponentiated efficiently [30]. For the kernel matrix \hat{K} and $\hat{\mathbb{1}}$ which are not sparse, we can use the technique of density matrix exponentiation with time cost of $O(\tau^2/\epsilon)$ [18]. (Note that we cannot exponentiate $X_i(A)$ directly using this method since $X_i(A)$ is not a density matrix. For simplicity, we assume that tensoring A with a qutrit operator to create $X_i(A)$ in the exponent can be done in constant time.) Hence, $e^{iX_3(\hat{K}\hat{\mathbb{1}})\tau}$ and automatically $e^{iX_3((\hat{K}\hat{\mathbb{1}})\otimes I)\tau}$ (since $e^{iA} \otimes I = e^{iA \otimes I}$) can be created efficiently via the multiplication subroutine.

B. Calculate the inverse of degree matrix

Having $e^{iX_3(D)t}$ already in the exponential form, it is natural to construct the inverse of D using quantum phase estimation (QPE) akin to the HHL algorithm for matrix inversion [25], with the following differences:

1. Our degree matrix is always well-conditioned, having all eigenvalues in the range $1 \leq d_i < N$.

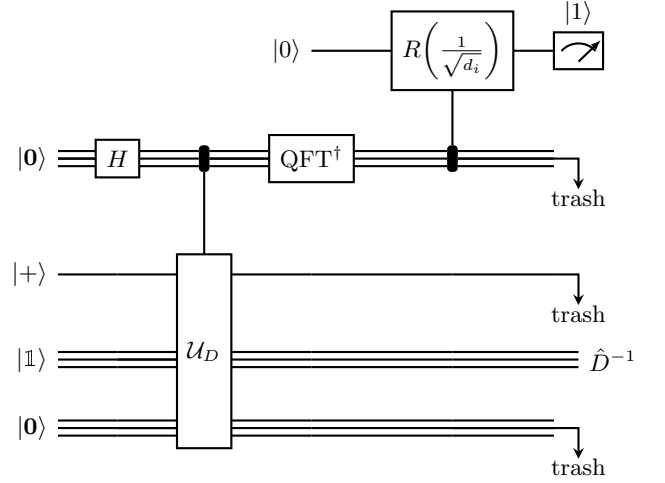


FIG. 3. Quantum circuit for degree matrix inversion

2. To construct the transition matrix, we would like the resulting inverse matrix in the form of a density matrix to be fed into the QMAT framework once more via density matrix exponentiation. Following [26], this implies that the function of the eigenvalues we want to compute is $1/\sqrt{d_i}$ instead of $1/d_i$.

The quantum circuit for the QPE is initialized in the state

$$|\psi_0\rangle = |\mathbf{0}\rangle \otimes |+\rangle \otimes |\mathbb{1}\rangle \otimes |\mathbf{0}\rangle, \quad (19)$$

where $|+\rangle = \frac{1}{\sqrt{2}}(|0\rangle + |2\rangle)$ and $|\mathbb{1}\rangle = \frac{1}{\sqrt{N}} \sum_{i=0}^{N-1} |i\rangle$. The first register will contain the estimated phase \tilde{d}_i associated to d_i after the QPE. The next two registers will contain the eigenvectors of $X_3(D)$, and the last one is added for collapsing other term except $e^{iX_3(D)t}$ in (18). Denote by $\kappa_D = d_{\max}/d_{\min}$ the condition number of D , i.e. the ratio of the largest eigenvalue to the smallest eigenvalue. Setting $t = O(\kappa_D^{0.5}/\epsilon)$ in the QPE results in the final state $\frac{1}{\sqrt{N}} \sum_{i=0}^{N-1} |\tilde{d}_i\rangle \otimes |+\rangle \otimes |i\rangle \otimes |\mathbf{0}\rangle$.

After the conditional rotation on the ancilla qubit, the state is

$$\sum_{i=0}^{N-1} \left(\sqrt{1 - \frac{\tilde{C}}{d_i}} |0\rangle + \sqrt{\frac{\tilde{C}}{d_i}} |1\rangle \right) \otimes |\tilde{d}_i\rangle \otimes |+\rangle \otimes |i\rangle \otimes |\mathbf{0}\rangle, \quad (20)$$

where \tilde{C} is of order $O(d_{\min})$. We then perform post-selection on the outcome “1” on the ancilla qubit and take the partial trace over the first, second, and last register to obtain

$$\hat{D}^{-1} = \tilde{C} \sum_{i=0}^{N-1} \frac{1}{d_i} |i\rangle\langle i|, \quad (21)$$

where $\tilde{C} = O\left(\left\{\sum_{i=0}^{N-1} d_i^{-1}\right\}^{-1}\right)$ with success probability $\Omega(1/\kappa_D)$ [26]. The success probability can be am-

plified to near certainty by repeating $O(\kappa_D^{0.5})$ rounds of amplitude amplification on the ancilla register [25]. Via another multiplication subroutine, we now have access to the transition matrix $P = D^{-1}K$.

V. EIGEN-DECOMPOSITION

The components of the diffusion map consist of the (right) eigenvectors and the eigenvalues of the transition matrix P , which we now extract by another QPE subroutine. Denote by $\{|u_i\rangle\}$, $\{|v_i\rangle\}$, and $\{\lambda_i\}$, the left eigenvectors, the right eigenvectors, and the corresponding eigenvalues of P respectively. The output of the QPE will be an estimate of the eigenvalues and the eigenvectors of

$$X_3(P) = R_3 \otimes P + R_3^\dagger \otimes P^\dagger = \begin{pmatrix} 0 & 0 & P \\ 0 & 0 & 0 \\ P^\dagger & 0 & 0 \end{pmatrix}, \quad (22)$$

which are $\{\pm\lambda_i\}_{i=0}^{N-1}$ and $|w_i^\pm\rangle = \frac{1}{\sqrt{2}}(|0\rangle \otimes |u_i\rangle \pm |2\rangle \otimes |v_i\rangle)$.

For an arbitrary $|\psi_0\rangle$, the input state $|0\rangle \otimes |\psi_0\rangle$ can be written as

$$|0\rangle \otimes |\psi_0\rangle = |0\rangle \otimes \sum_{i=0}^{N-1} \frac{\beta_i}{\sqrt{2}} (|w_i^+\rangle + |w_i^-\rangle) \quad (23)$$

for some $\{\beta_i\}$. The output state of the QPE after evolving for time t is

$$\sum_{i=0}^{N-1} \frac{\beta_i}{\sqrt{2}} \left(\left| \frac{\widetilde{\lambda_i t}}{2\pi} \right\rangle \otimes |w_i^+\rangle + \left| -\frac{\widetilde{\lambda_i t}}{2\pi} \right\rangle \otimes |w_i^-\rangle \right), \quad (24)$$

where tilde denotes the binary representation of the phases in the range $[0, 2\pi)$. ($-x$ is the 2-complement of \tilde{x} .) In order to distinguish the positive and negative eigenvalues, we set $t = \pi$ so that $-\widetilde{\lambda_i/2}$ only take values greater than $0.1\dots$ (or 0.5 in the decimal representation), giving the state

$$\sum_{i=0}^{N-1} \frac{\beta_i}{\sqrt{2}} \left(\left| \frac{\widetilde{\lambda_i}}{2} \right\rangle \otimes |w_i^+\rangle + \left| -\frac{\widetilde{\lambda_i}}{2} \right\rangle \otimes |w_i^-\rangle \right). \quad (25)$$

We describe in the next section how to extract from this quantum state the desired eigenvalues (only the $\lambda_i/2$ terms) and eigenvectors (only the right eigenvectors $|v_i\rangle$).

A. Extracting desired eigenvalues and eigenvectors

Previously, we have the estimated phases from the QPE in (25), where the desired eigenvalues and eigenvectors are only positive eigenvalues $\left| \frac{\widetilde{\lambda_i}}{2} \right\rangle$ and $|v_i\rangle$. To extract them, we can use amplitude amplification (AA)

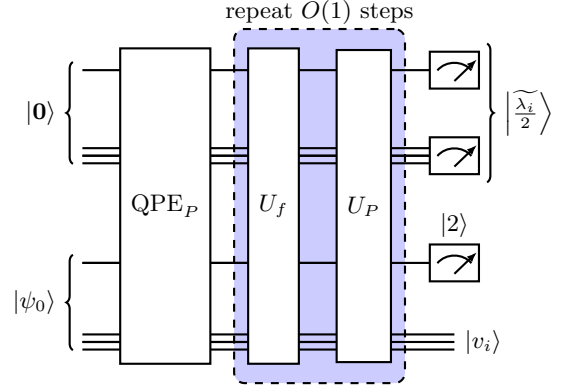


FIG. 4. Quantum circuit demonstration for eigen-extraction

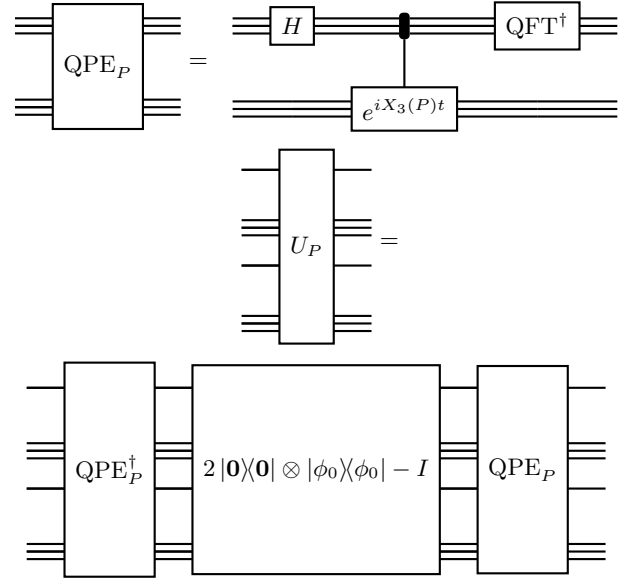


FIG. 5. Gates expansion of Fig. 4

algorithm to amplify the amplitudes corresponding to those desired quantum states. The amplitude amplification is based on Grover's search algorithm. In AA, define a unitary operator $Q = U_P U_f$, where U_f negates amplitudes of the marked quantum states and U_P amplifies those marked quantum states. In our case, the marked states correspond to the positive non-unity eigenvalues and their right eigenvectors $|v_i\rangle$. For the positive non-unity eigenvalues, the first qubit in the eigenvalues register must be $|0\rangle$, and for the right eigenvectors, the qubit in the eigenvectors register must be $|2\rangle$. We thus construct the operator U_f for negating marked states as

$$U_f = I - 2(|0\rangle\langle 0| \otimes I \otimes |2\rangle\langle 2| \otimes I). \quad (26)$$

The Grover diffusion operator U_P is defined as $U_P = 2|\psi\rangle\langle\psi| - I$, where $|\psi\rangle = \text{QPE}(|0\rangle \otimes |\psi_0\rangle)$ is the state (25) after the QPE. We thus have that

$$U_P = \text{QPE}(2(|0\rangle\langle 0| \otimes |\psi_0\rangle\langle\psi_0|) - I)\text{QPE}^\dagger. \quad (27)$$

Algorithm 1: Quantum diffusion map

Input : Classical data X
Output: Eigenvalues $\{\lambda_i\}$ and right eigenvectors $\{v_i\}$ of the Markov transition matrix P

1. Embed X into coherent state qRAM
 2. Perform partial trace to obtain \hat{K}
 3. Create state $\hat{1}$ and construct $e^{iX_1(\hat{K})t}$ and $e^{iX_2(\hat{1})t}$
 4. Construct $e^{iX_3(D)t}$ where $t = O(\kappa_D^{0.5}/\epsilon_D)$
 5. Invert D by
 - (a) Using $e^{iX_3(D)t}$ in QPE initialized using state (19)
 - (b) Rotating the ancilla qubit controlled by eigenvalues register
 - (c) Amplifying an ancilla qubit “1” and perform partial trace on the first two and last registers to get \hat{D}^{-1}
 6. Construct $e^{iX_3(\hat{D}^{-1})t}$ and $e^{iX_3(P)t}$ where $t = O(1/\epsilon_P)$
 7. Use $e^{iX_3(P)t}$ in QPE initialized using state (23)
 8. Amplify and measure a λ_i register to get an approximated λ_i
 9. Use tomography to get an v_i corresponding to the λ_i measured in 8.
-

We then repeat Q in $O(1)$ steps (shown in Appendix B 4). After we measure the first qubit of the eigenvector register, the state will be $\sum_{i=1}^{N-1} \beta_i \left| \frac{\lambda_i}{2} \right\rangle \otimes |v_i\rangle$, which contains all the desired eigenvalues and eigenvectors of transition matrix.

Measuring the eigenvalue register gives one of the halved eigenvalues and collapses the other register to the eigenvector corresponding to that eigenvalue (assuming no degeneracy as in the classical case (Sec. II A)). The eigenvector can then be extracted using a number of copies that scales almost linearly in N [31]. Repeating the procedure for (at most) $N - 1$ eigenvalues and eigenvectors allow us to classically construct the diffusion map (5).

VI. TIME COMPLEXITY OF QUANTUM DIFFUSION MAP

The complexity of qDM is summarized in Theorem 1, the proof of which is provided in Appendix B.

Theorem 1 (time complexity of qDM) *For a dataset $X = \{\mathbf{x}^{(i)}\}_{i=0}^{N-1}$ such that each $\mathbf{x}^{(i)} \in \mathbb{R}^d$ and $d < N$, the quantum diffusion map in Algorithm 1 can*

be implemented with a runtime of

$$O\left(\frac{N^2}{\epsilon_t \epsilon_P^2 \epsilon_e} \left(\left(\frac{\kappa_D^{1.25}}{\epsilon_D^{1.5} \epsilon_m^{0.5}} + \frac{\kappa_D^{1.125}}{\epsilon_D^{1.25} \epsilon_m^{0.75} \epsilon_e} \right) \log^4 N + \log^3 N \right)\right), \quad (28)$$

where κ_D denotes the condition number of the degree matrix D , and each ϵ with subscript denotes the error of the following subroutines: “e” for the density matrix exponentiation, “m” for the matrix multiplication subroutine, “D” for the degree matrix inversion, “P” for the eigenvalue estimation, and “t” for quantum tomography.

When the errors and the condition number are independent of the dataset size N , the complexity reduces to

$$O(N^2 \text{polylog } N), \quad (29)$$

achieving a speedup compared to the classical diffusion map algorithm which requires $O(N^3)$ time. In fact, the bottleneck of $\tilde{O}(N^2)$ solely arises from the readout (tomography) alone (see Appendix B), which perhaps can be circumvented if one coherently outputs the diffusion map as quantum states, providing an end-to-end computation. Note that the fact that errors are independent of N are discussed in Appendix A and B. Also note that the condition number of the degree matrix depends on the neighborhood connectivity of the dataset, which shall be tuned to be $O(1)$ and independent of N , provided the scale of the neighborhood controlled by σ in the Kernel matrix is local, such as in Fig. 1 (middle).

VII. DISCUSSION AND CONCLUSION

In this work, we first review classical diffusion map, an unsupervised learning algorithm for nonlinear dimensionality reduction and manifold learning. We then explain our efforts to construct quantum algorithm for diffusion map. Our quantum diffusion map (qDM) consists of 5 major steps: coherent state data encoding scheme, a natural construction of kernel matrix from coherent states, a scheme to construct the Markov transition operator from the kernel matrix, the eigen-decomposition of the transition operator, and extracting relevant quantum information to construct diffusion map classically. The time complexity of qDM is $O(N^2 \text{polylog } N)$, providing a computational speedup over a classical DM whose time complexity is $O(N^3)$. Importantly, from encoding classical data to performing an eigen-decomposition of the Markov transition operator, the total time complexity is only $O(\log^3 N)$. Such exponential speedup for transition operator construction and analysis could be useful in many random walk-based algorithms.

Regarding the $\tilde{O}(N^2)$ bottleneck, a method to sort the eigenvalues and select only the top ones would reduce the complexity. Alternatively, one could devise a qDM algorithm that outputs the eigenvectors as quantum states and retain the exponential speedup. We leave open the

question of how one could make use of such state for nonlinear dimensionality reduction.

Recently, manipulation of matrices and their spectra by block-encoding into submatrices of unitary matrices has become a topic of great interest due to its versatility in quantum algorithm design [32, 33], which may provide an alternative route to qDM algorithm.

ACKNOWLEDGMENTS

A.S. especially thanks Dimitris Angelakis from the Centre for Quantum Technologies (CQT), Singapore, for hospitality, and for useful advice on quantum algorithms. We also thank Jirawat Tangpanitanon and Supanut Thanasilp for useful discussions. This research is supported by the Program Management Unit for Human Resources and Institutional Development, Research and Innovation (grant number B05F630108), and Sci-Super VI fund from the faculty of science, Chulalongkorn University.

-
- [1] J. B. Tenenbaum, V. d. Silva, and J. C. Langford, A global geometric framework for nonlinear dimensionality reduction, *Science* **290**, 2319 (2000).
- [2] M. Belkin and P. Niyogi, Laplacian eigenmaps and spectral techniques for embedding and clustering, in *Adv. Neural Inf. Process. Syst.* **14** (MIT Press, 2001) pp. 585–591.
- [3] L. McInnes, J. Healy, N. Saul, and L. Großberger, UMAP: Uniform manifold approximation and projection, *J. Open Source Softw.* **3**, 861 (2018).
- [4] M. Scholz, F. Kaplan, C. L. Guy, J. Kopka, and J. Selbig, Non-linear PCA: a missing data approach, *Bioinformatics* **21**, 3887 (2005).
- [5] L. van der Maaten and G. Hinton, Visualizing data using t-SNE, *J. Mach. Learn. Res.* **9**, 2579 (2008).
- [6] R. R. Coifman and S. Lafon, Diffusion maps, *Appl. Comput. Harmon. Anal.* **21**, 5 (2006).
- [7] S. Lafon, *Diffusion maps and geometric harmonics*, Ph.D. thesis, Yale University (2004).
- [8] B. Nadler, S. Lafon, I. Kevrekidis, and R. Coifman, Diffusion maps, spectral clustering and eigenfunctions of Fokker-Planck operators, in *Adv. Neural Inf. Process. Syst.*, Vol. 18, edited by Y. Weiss, B. Schölkopf, and J. Platt (MIT Press, 2006).
- [9] K. R. Moon, D. van Dijk, Z. Wang, S. Gigante, D. B. Burkhardt, W. S. Chen, K. Yim, A. van den Elzen, M. J. Hirn, R. R. Coifman, N. B. Ivanova, G. Wolf, and S. Krishnaswamy, Visualizing structure and transitions in high-dimensional biological data, *Nat. Biotechnol.* **37**, 1482 (2019).
- [10] C. L. Ecale Zhou, S. Malfatti, J. Kimbrel, C. Philipson, K. McNair, T. Hamilton, R. Edwards, and B. Souza, multiPhATE: bioinformatics pipeline for functional annotation of phage isolates, *Bioinformatics* **35**, 4402 (2019).
- [11] J. F. Rodriguez-Nieva and M. S. Scheurer, Identifying topological order through unsupervised machine learning, *Nat. Phys.* **15**, 790 (2019).
- [12] Y. Long, J. Ren, and H. Chen, Unsupervised manifold clustering of topological phononics, *Phys. Rev. Lett.* **124**, 185501 (2020).
- [13] A. Lidiak and Z. Gong, Unsupervised machine learning of quantum phase transitions using diffusion maps, *Phys. Rev. Lett.* **125**, 225701 (2020).
- [14] A. Kerr, G. Jose, C. Riggert, and K. Mullen, Automatic learning of topological phase boundaries, *Phys. Rev. E* **103**, 023310 (2021).
- [15] Y. Che, C. Gneiting, T. Liu, and F. Nori, Topological quantum phase transitions retrieved through unsupervised machine learning, *Phys. Rev. B* **102**, 134213 (2020).
- [16] J. Wang, W. Zhang, T. Hua, and T.-C. Wei, Unsupervised learning of topological phase transitions using the Calinski-Harabaz index, *Phys. Rev. Research* **3**, 013074 (2021).
- [17] P. Reberntrost, A. Steffens, I. Marvian, and S. Lloyd, Quantum singular-value decomposition of nonsparse low-rank matrices, *Phys. Rev. A* **97**, 012327 (2018).
- [18] S. Lloyd, M. Mohseni, and P. Reberntrost, Quantum principal component analysis, *Nat. Phys.* **10**, 631 (2014).
- [19] S. Apers and R. de Wolf, Quantum speedup for graph sparsification, cut approximation and laplacian solving, in *Proc. IEEE 61st Annu. Symp. Found. Comput. Science (FOCS)* (2020) pp. 637–648.
- [20] I. Kerenidis and J. Landman, Quantum spectral clustering, *Phys. Rev. A* **103**, 042415 (2021).
- [21] I. Kerenidis, J. Landman, A. Luongo, and A. Prakash, q-means: A quantum algorithm for unsupervised machine learning, in *Adv. Neural Inf. Process. Syst.*, Vol. 32, edited by H. Wallach, H. Larochelle, A. Beygelzimer, F. d'Alché-Buc, E. Fox, and R. Garnett (Curran Associates, 2019).
- [22] D. Dua and C. Graff, *UCI machine learning repository* (2017).
- [23] L. N. Trefethen and D. Bau III, *Numerical linear algebra*, Vol. 50 (Siam, 1997).
- [24] L. Zhao, Z. Zhao, P. Reberntrost, and J. Fitzsimons, Compiling basic linear algebra subroutines for quantum computers, *arXiv:1902.10394* (2019).
- [25] A. W. Harrow, A. Hassidim, and S. Lloyd, Quantum algorithm for linear systems of equations, *Phys. Rev. Lett.* **103**, 150502 (2009).
- [26] I. Cong and L. Duan, Quantum discriminant analysis for dimensionality reduction and classification, *New J. Phys.* **18**, 073011 (2016).
- [27] G. H. Low and I. L. Chuang, Optimal hamiltonian simulation by quantum signal processing, *Phys. Rev. Lett.* **118**, 010501 (2017).
- [28] R. Chatterjee and T. Yu, Generalized coherent states, reproducing kernels, and quantum support vector machines, *Quantum Info. Comput.* **17**, 1292–1306 (2017).
- [29] V. Giovannetti, S. Lloyd, and L. Maccone, Quantum random access memory, *Phys. Rev. Lett.* **100**, 160501 (2008).
- [30] An $N \times N$ matrix is s -sparse if there are at most s nonzero

entries per row. An $N \times N$ matrix is *sparse* if it is at most $\text{polylog}(N)$ -sparse.

- [31] I. Kerenidis and A. Prakash, A quantum interior point method for lps and sdps, *ACM Trans. Quantum Comput.* **1**, 1 (2020).
- [32] A. Gilyén, Y. Su, G. H. Low, and N. Wiebe, Quantum singular value transformation and beyond: Exponential improvements for quantum matrix arithmetics, in *Proc. 51st Annu. ACM SIGACT Symp. Theor. Comput.*, STOC 2019 (Association for Computing Machinery, New York, NY, USA, 2019) p. 193–204.
- [33] J. M. Martyn, Z. M. Rossi, A. K. Tan, and I. L. Chuang, A grand unification of quantum algorithms, *arXiv:2105.02859* (2021).
- [34] P. Rebentrost, M. Mohseni, and S. Lloyd, Quantum support vector machine for big data classification, *Phys. Rev. Lett.* **113**, 130503 (2014).
- [35] D. Dervovic, M. Herbster, P. Mountney, S. Severini, N. Usher, and L. Wossnig, Quantum linear systems algorithms: a primer, *arXiv:1802.08227* (2018).

Appendix A: QMAT matrix multiplication subroutine

As explained in Sec. IV A, all QMAT subroutines [24] utilized in our work reduce to that of matrix multiplication, which we now describe. Given matrices A_1 and A_2 , the idea of the multiplication subroutine is to construct a Hermitian embedding of the product $A_1 A_2$,

$$X_3(A_1 A_2) = \begin{pmatrix} 0 & 0 & A_1 A_2 \\ 0 & 0 & 0 \\ (A_1 A_2)^\dagger & 0 & 0 \end{pmatrix},$$

from the following commutator:

$$X_3(A_1 A_2) = U X_3(i A_1 A_2) U^\dagger = i U [X_1(A_1), X_2(A_2)] U^\dagger, \quad (\text{A1})$$

where

$$U = \begin{pmatrix} \sqrt{-i} I & 0 & 0 \\ 0 & I & 0 \\ 0 & 0 & \sqrt{i} I \end{pmatrix}.$$

Thus, the goal is to simulate the commutator of two hermitian operators. This can be accomplished with bounded error via the second order of the Baker-Campbell-Hausdorff formula. Define

$$\tilde{l}(x, y) \equiv e^x e^y e^{-x} e^{-y} e^{-x} e^{-y} e^x e^y.$$

With the step size t/m , we have that [24],

$$\tilde{l}(xt/m, yt/m) = e^{2[x, y]t^2/m^2 + O(t^4/m^4)}. \quad (\text{A2})$$

Thus, iterating the above $n' = m^2/(2t) = O(t^2/\epsilon_m)$ times,

$$\tilde{l}(xt/m, yt/m)^{n^2/(2t)} = e^{[x, y]t + O(t^3/m^2)}, \quad (\text{A3})$$

correctly simulates $e^{[x, y]t}$ up to an error $\epsilon_m = O(t^3/m^2)$.

Putting all these together, the QMAT multiplication subroutine consumes $n' = m^2/(2t)$ copies of $e^{iX_1(A_1)t/m}$ and $e^{iX_2(A_2)t/m}$ (and their inverses), and outputs a unitary operator

$$U[l(iX_1(A_1)t/m, iX_2(A_2)t/m)]^{n'} U^\dagger, \quad (\text{A4})$$

that approximates $e^{iX_3(A_1 A_2)}$ up to an error ϵ_m in the operator norm.

Appendix B: Complexity analysis

This section describes the calculation for the time complexity that leads to the result in Theorem 1. We separate the algorithm into sequential steps as we have done with the classical DM (Sec. II B), namely, the embedding of classical data into the kernel \hat{K} , the calculation of the transition matrix P , and the calculation of the eigendecomposition. We also include the complexity analysis of the amplitude amplification algorithm, which we use to improve the probabilities of certain outcomes from our algorithm.

1. Preparing the kernel

In creating \hat{K} , we consider only the time complexity coming from storing classical data into qRAM (Sec. III A) as partial trace does not create additional time cost. Assuming that the data consists of N vectors each with d features, the data can be encoded into a qRAM of the size dN , which can be accessed using $O(\log(dN))$ operations (11) [34]. We assume here that we are dealing with big data, i.e., $d \leq N$. Therefore, the time cost becomes $O(\log N^2) = O(\log N)$.

2. Calculating the transition matrix

Next, we construct the exponential of P . We start with exponentiating the necessary matrices. Then we multiply these matrices in order to create $e^{iX_3(D)t}$. Next, we inverse the degree matrix D before constructing the transition matrix $P = D^{-1}K$.

The time cost of creating exponentials depends on whether the quantum simulation of matrices or quantum state is used. Creating exponentials from multiple copies of density matrices, i.e., $e^{iX_3(\hat{K})t}$ and $e^{iX_3(\hat{1})t}$, results in a time complexity of $O(t^2/\epsilon_e)$, where ϵ_e is the accuracy for the exponentiation [18]. Combined with the number of operations for storing the states, which is $O(\log N)$, the time complexity is $O(t^2/\epsilon_e \log N)$.

Exponentials of sparse matrices can be simulated using the method in [27] with query complexity of $O\left(t + \frac{\log(1/\epsilon_s)}{\log \log(1/\epsilon_s)}\right)$, where ϵ_s is the accuracy of the method. For the matrices $e^{iX_3(\Xi)t}$ and $e^{iX_3(\Xi^\dagger)t}$, we also

need to take into account the gate complexity $O(\log N)$. Thus the time complexity for preparing each of these exponentials is $O(t \log N)$.

To construct the degree matrix, we use the matrix multiplication subroutine in Appendix A. This subroutine uses 4 copies of each input exponential, which is multiplied and then applied n' times. In creating $e^{iX_3(\hat{K} \otimes I)}$ (Sec. IV A), the time cost comes from multiplying the exponential of \hat{K} and of $\mathbb{1}$ whereas $\otimes I$ is assumed to be a free operation. Therefore, the time cost is $O\left(n' \left(\frac{t^2}{m^2 \epsilon_e} \log N\right)\right)$. Given the condition that $n' = \frac{m^2}{2t} = O\left(\frac{t^2}{\epsilon_m}\right)$ [24], we rewrite the time cost to $O(t \log N \epsilon_e^{-1})$.

In the next two steps, we multiply Ξ and Ξ^\dagger into $K \mathbb{1} \otimes I$. Again, we apply the multiplication subroutine iteratively with 4 copies of the result from the previous multiplication as one of the input. These steps admit additional order of ϵ_m and t which leads the time cost of $e^{iX_3(D)t}$ to be

$$T_D = O\left(\left(\frac{t^{1.5}}{\epsilon_m^{0.5}} + \frac{t^{1.25}}{\epsilon_e \epsilon_m^{0.75}}\right) \log N\right). \quad (\text{B1})$$

Next, the degree matrix D is inverted (Sec. IV B) by first performing QPE that takes the prepared $e^{iX_3(D)t}$ as the unitary operator in QPE then a controlled rotation. The time cost of the QPE is $O(T_D/\epsilon_D \log m)$ [35], where m is the number of eigenvalues which is $m = N$, and ϵ_D is the error of estimated phase. Assuming the controlled rotation is executed in time $O(1)$, we have accumulated a time cost of $T_D + O(T_D/\epsilon_D \log N) + O(1)$. The time complexity is thus dominated by $O(T_D/\epsilon_D \log N)$.

The time T_D (B1) is a function of t , which we now find through error analysis of matrix inversion. As we are inverting the eigenvalues of D to a function of $1/\sqrt{x}$ [26], the error after conditioned rotation becomes $\epsilon_D = O(1/\sqrt{d_i t}) < O(\kappa_D^{0.5}/t)$. Thus the time is $t = O(\kappa_D^{0.5}/\epsilon_D)$.

As the success probability of measuring $|1\rangle$ in the ancilla qubit is $\Omega(1/\kappa_D)$, the number of rounds necessary to obtain a successful result is $O(\kappa_D)$. To accelerate the process, we use the amplitude amplification to amplify the success probability in $O(\kappa_D^{0.5})$ steps. Thus an overall complexity becomes

$$T_{D^{-1}} = O\left(\left(\frac{\kappa_D^{1.25}}{\epsilon_D^{1.5} \epsilon_m^{0.5}} + \frac{\kappa_D^{1.125}}{\epsilon_D^{1.25} \epsilon_e \epsilon_m^{0.75}}\right) \log^2 N\right). \quad (\text{B2})$$

The last step in constructing the transition matrix is multiplying inverse degree matrix to \hat{K} , which we perform this multiplication in the exponential (Sec. IV B). Therefore, we first need to exponentiate D^{-1} and \hat{K} using a time of $O(t^2/(n^2 \epsilon_e))$ and $4n'$ copies each. The time complexity for constructing $e^{iX_3(P)t}$ is therefore

$$O\left(\left(\frac{\kappa_D^{1.25}}{\epsilon_D^{1.5} \epsilon_m^{0.5}} + \frac{\kappa_D^{1.125}}{\epsilon_D^{1.25} \epsilon_m^{0.75} \epsilon_e}\right) \frac{t \log^2 N}{\epsilon_e} + \frac{t \log N}{\epsilon_e}\right).$$

3. Eigen-decomposition

In this subsection, we find the eigenvalues and eigenvectors of P , using a second QPE algorithm (Sec. V). We take $t = O(1/\epsilon_P)$ to perform the QPE in time $O(\log N)$ with accuracy ϵ_P [35], and then perform the amplitude amplification. In this step, the number of rounds used in amplitude amplification is in $O(1)$ (Appendix B 4) as the number of rounds depends on the input state to the amplification algorithm and not the matrix P .

The process of obtaining each copy of the eigenvector is not deterministic, and we could use amplitude amplification to amplify such probability. However the number of rounds of amplitude amplification does not depend explicitly on N and thus we ignore it in our analysis.

We extract all desired eigenpairs by repeating the QPE and the amplitude amplification for each eigenpair, leading to an $O(N)$ rounds (searching $N - 1$ terms from $4N$ terms in (25)). Then the pure-state tomography algorithm of [31] recovers a classical vector that is ϵ_t -close in ℓ_2 -norm to the eigenvector using $O(N \log N/\epsilon_t)$ copies. Thus, the overall complexity of qDM becomes

$$O\left(\left(\frac{\kappa_D^{1.25}}{\epsilon_D^{1.5} \epsilon_m^{0.5}} + \frac{\kappa_D^{1.125}}{\epsilon_D^{1.25} \epsilon_m^{0.75} \epsilon_e}\right) \frac{N^2 \log^4 N}{\epsilon_P^2 \epsilon_e \epsilon_t} + \frac{N^2 \log^3 N}{\epsilon_P^2 \epsilon_e \epsilon_t}\right).$$

This proves Theorem 1.

4. Complexity of amplitude amplification

In Section V A, we use AA to amplify the amplitudes in the desired subspace. Referring to the state (25), we define the ‘‘good’’ subspace to be spanned by $|0\rangle$ in the register that contains the most significant bit of the estimated phases, and $|2\rangle$ in the register that labels whether the eigenvectors are the left or the right eigenvectors. That is, we are amplifying only the terms corresponding to positive eigenvalues $\tilde{\lambda}_i/2$ and the right eigenvectors. Let T be the projector onto the good subspace. We then have that

$$\begin{aligned} |\psi\rangle &= T|\psi\rangle + (I - T)|\psi\rangle \\ &= \sin\theta |\psi_G\rangle + \cos\theta |\psi_G^\perp\rangle, \end{aligned} \quad (\text{B3})$$

where $\sin\theta = \|T|\psi\rangle\|_2$ is the amplitude in the good subspace, and $|\psi_G\rangle$ and $|\psi_G^\perp\rangle$ are normalized vectors in the good subspace and its complement respectively. By a straightforward calculation, we have that

$$\sin\theta = \sqrt{\frac{1}{4} \left(\sum_{i=0}^{N-1} \beta_i^2 - \beta_0^2 \right)} = \sqrt{\frac{1}{4} (1 - \beta_0^2)} = O(1). \quad (\text{B4})$$

Since the number of repetitions required for AA is $\lceil \frac{\pi}{4\theta} \rceil$, we have that $O(1)$ repetitions suffice, implying that the number of repetitions is also constant.